Acoustic Force Density Acting on Inhomogeneous Fluids in Acoustic Fields

Jonas T. Karlsen,[1,*] Per Augustsson,[2] and Henrik Bruus[1,†]

[1]*Department of Physics, Technical University of Denmark, DTU Physics Building 309, DK-2800 Kongens Lyngby, Denmark*
[2]*Department of Biomedical Engineering, Lund University, Ole Römers väg 3, 22363 Lund, Sweden*

We present a theory for the acoustic force density acting on inhomogeneous fluids in acoustic fields on time scales that are slow compared to the acoustic oscillation period. The acoustic force density depends on gradients in the density and compressibility of the fluid. For microfluidic systems, the theory predicts a relocation of the inhomogeneities into stable field-dependent configurations, which are qualitatively different from the horizontally layered configurations due to gravity. Experimental validation is obtained by confocal imaging of aqueous solutions in a glass-silicon microchip.

The physics of acoustic forces on fluids and suspensions has a long and rich history including early work on fundamental phenomena such as acoustic streaming [1–4], the acoustic radiation force acting on a particle [5,6] or an interface of two immiscible fluids [7], and acoustic levitation [8,9]. Driven by applications related to particle and droplet handling, the field continues to be active with recent advanced studies of acoustic levitators [10–12], acoustic tweezers and tractor beams [13–15], thermoviscous effects [16–18], and, in general, rapid advances within the field of microscale acoustofluidics [19]. In the latter, acoustic radiation forces are used to confine, separate, sort, or probe particles such as microvesicles [20,21], cells [22–26], bacteria [27,28], and biomolecules [29]. Biomedical applications include the early detection of circulating tumor cells in blood [30,31] and the diagnosis of bloodstream infections [32].

The theoretical treatment of acoustic forces involves nonlinear models including multiple length and time scales [33]. Steady acoustic streaming [34] describes a steady swirling fluid motion, spawned by fast-time-scale acoustic dissipation either in boundary layers [2] or in the bulk [3]. Similarly, the acoustic radiation force acting on a particle [18] or an interface of two immiscible fluids [35,36] is due to interactions between the incident and the scattered acoustic waves. This force derives from a divergence in the time-averaged momentum-flux-density tensor, which is nonzero only at the position of the particle or the interface.

Recently, in microchannel acoustofluidics experiments, it was discovered that acoustic forces can relocate inhomogeneous aqueous salt solutions and stabilize the resulting density profiles against hydrostatic pressure gradients [37]. Building on this discovery, isoacoustic focusing was subsequently introduced as an equilibrium cell-handling method that overcomes the central issue of cell-size dependency in acoustophoresis [38]. The method can be considered a microfluidic analog to density gradient centrifugation, achieving spatial separation of different cell types based on differences in their acoustomechanical properties. Not surprisingly, the subtle nonlinear acoustic phenomenon of relocation and stabilization of inhomogeneous fluids was discovered in the realm of microfluidics, where typical hydrostatic pressure differences ($\sim$1 Pa) are comparable to, or less than, the acoustic energy densities (1–100 Pa) obtained in typical microchannel resonators [38–40].

The main goal of this Letter is to provide a theoretical explanation of this phenomenon. To this end, we extend acoustic radiation force theory beyond the requirement of immiscible phases, and we present a general theory for the time-averaged acoustic force density acting on a fluid with a continuous spatial variation in density and compressibility. The starting point of our treatment is to identify and exploit the separation in time scales between the fast time scale of acoustic oscillations and the slow time scale of the oscillation-time-averaged fluid motion. We show that gradients in density and compressibility result in a divergence in the time-averaged momentum-flux-density tensor, which, in contrast to the case of immiscible phases, is generally nonzero everywhere in space. Our theory explains the observed relocation and stabilization of inhomogeneous fluids. Furthermore, we present an experimental validation of our theory obtained by confocal imaging in an acoustofluidic glass-silicon microchip.

Characteristic time scales.—Consider the sketch in Fig. 1 of a long, straight microchannel of cross-sectional width $W = 375\ \mu$m and height $H = 150\ \mu$m filled with a fluid of inhomogeneous density $\rho_0(\boldsymbol{r}) = [1 + \hat{\rho}(\boldsymbol{r})]\rho_0^{(0)}$, adiabatic compressibility $\kappa_0(\boldsymbol{r})$, and dynamic viscosity $\eta_0(\boldsymbol{r})$. Here, $\hat{\rho}(\boldsymbol{r})$ is the relative deviation away from the reference density $\rho_0^{(0)}$. Assuming an acoustic standing half-wave resonance at angular frequency ω, the wave number is $k = \omega/c = \pi/W$, where $c = 1/\sqrt{\rho_0 \kappa_0}$ is the speed of sound. In terms of the parameters of the microchannel and of water at ambient conditions, the fast acoustic oscillation time scale t is
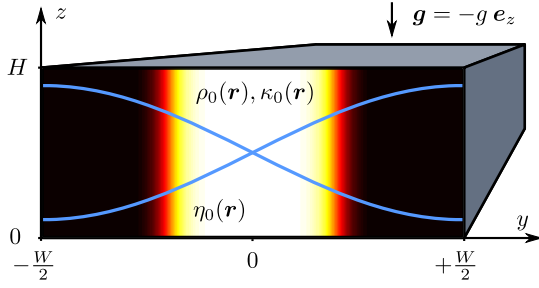
FIG. 1.   Sketch of a long, straight acoustofluidic microchannel of length $L = 40$ mm along x, width $W = 375$ μm and height $H = 150$ μm with an imposed half-wave acoustic pressure resonance (sinusoidal curves) inside a glass-silicon chip. A salt concentration (black, low; white, high) leads to an inhomogeneous-fluid density $\rho_0(\mathbf{r})$, compressibility $\kappa_0(\mathbf{r})$, and dynamic viscosity $\eta_0(\mathbf{r})$. The gravitational acceleration is $\mathbf{g} = -g\mathbf{e}_z$.

$$t \sim \frac{1}{\omega} = \frac{1}{kc} = \frac{1}{\pi} W \sqrt{\rho_0 \kappa_0} \sim 0.1 \ \mu\text{s}. \qquad (1)$$

In contrast, the time scales associated with flows driven by hydrostatic pressure gradients are much slower. Given the length scale H, the gravitational acceleration g, and the kinematic viscosity $\nu_0 = \eta_0/\rho_0$, we estimate the time scale of inertia $t_{\text{inertia}} \sim \sqrt{H/(g\hat{\rho})}$, of viscous relaxation $t_{\text{relax}} \sim H^2/\nu_0$, and of steady shear motion $t_{\text{shear}} \sim \nu_0/(Hg\hat{\rho})$, with the latter being obtained by balancing the shear stress η_0/t_{shear} with the hydrostatic pressure difference $H\rho_0 g\hat{\rho}$. Remarkably, in our system with $\hat{\rho} \approx 0.1$, all time scales are of the order of 10 ms, henceforth denoted as the slow time scale τ,

$$\tau \sim t_{\text{inertia}} \sim t_{\text{relax}} \sim t_{\text{shear}} \sim 10 \ \text{ms}. \qquad (2)$$

Furthermore, for acoustic energy densities E_{ac} of the order $\rho_0 g H$, the time scale of flows driven by time-averaged acoustic forces is also τ. Hence, we have identified a separation of time scales into a fast acoustic time scale t and a slow time scale $\tau \sim 10^5 t$. This separation is sufficient to ensure $\tau \gg t$ in general, even for large variations in parameter values.

Fast-time-scale dynamics.—The dynamics at the fast time scale t describes acoustics for which viscosity may be neglected [41–43]. On this time scale ρ_0, κ_0, and η_0 can be assumed to be stationary, and the acoustic fields are treated as time-harmonic perturbations at the angular frequency ω [43]. The perturbation expansion for the density ρ thus takes the form

$$\rho = \rho_0(\mathbf{r}, \tau) + \rho_1(\mathbf{r}, \tau)e^{-i\omega t}, \qquad (3)$$

and likewise for the pressure p and the velocity $\mathbf{v}$. In terms of the material derivative $(d/dt) = \partial_t + (\mathbf{v} \cdot \boldsymbol{\nabla})$, the density-pressure relation for a fluid particle is

$$\frac{d\rho}{dt} = \frac{1}{c^2} \frac{dp}{dt}, \quad \text{where} \ \frac{1}{c^2} = \left(\frac{\partial\rho}{\partial p}\right)_S = \rho_0\kappa_0. \qquad (4)$$

Here, c is the adiabatic local speed of sound, which depends on the position through the inhomogeneity in κ_0 and ρ_0. Combining Eqs. (3) and (4) leads to the first-order relation

$$\partial_t\rho_1 + (\mathbf{v}_1 \cdot \boldsymbol{\nabla})\rho_0 = \rho_0\kappa_0[\partial_t p_1 + (\mathbf{v}_1 \cdot \boldsymbol{\nabla})p_0], \qquad (5)$$

where we have discarded terms involving $\mathbf{v}_0$, as they are negligible for $|\mathbf{v}_0| \ll c$. From the governing equations for mass and momentum [41–43] follows $|\boldsymbol{\nabla}p_0| \ll c^2|\boldsymbol{\nabla}\rho_0|$, and the term involving $\boldsymbol{\nabla}p_0$ in Eq. (5) is also negligible. This results in the first-order equations

$$\kappa_0\partial_t p_1 = -\boldsymbol{\nabla} \cdot \mathbf{v}_1, \qquad (6a)$$

$$\rho_0\partial_t\mathbf{v}_1 = -\boldsymbol{\nabla}p_1, \qquad (6b)$$

and the wave equation for the acoustic pressure p_1 in an inhomogeneous fluid [42,44],

$$\frac{1}{c^2}\partial_t^2 p_1 = \rho_0\boldsymbol{\nabla} \cdot \left[\frac{1}{\rho_0}\boldsymbol{\nabla}p_1\right]. \qquad (7)$$

Note that the curl of Eq. (6b) yields $\boldsymbol{\nabla} \times (\rho_0\mathbf{v}_1) = \mathbf{0}$, which implies that acoustics in inhomogeneous fluids should be formulated in terms of the mass current potential ϕ_ρ instead of the usual velocity potential,

$$\rho_0\mathbf{v}_1 = \boldsymbol{\nabla}\phi_\rho \quad \text{and} \quad p_1 = -\partial_t\phi_\rho. \qquad (8)$$

Combining Eqs. (6a) and (8) reveals that the mass current potential ϕ_ρ fulfills the same wave equation as p_1.

The acoustic force density.—The first-order acoustic fields lead to no net fluid displacement since the time average $\langle g_1 \rangle = (1/T)\int_0^T g_1 dt$ over one oscillation period T of any time-harmonic first-order field g_1 is zero. The description of time-averaged effects thus requires the solution of the time-averaged second-order equations, and the introduction of the time-averaged acoustic momentum-flux-density tensor $\langle \boldsymbol{\Pi} \rangle$ [41],

$$\langle \boldsymbol{\Pi} \rangle = \langle p_2 \rangle\mathbf{I} + \langle \rho_0\mathbf{v}_1\mathbf{v}_1 \rangle. \qquad (9)$$

Here, $\mathbf{I}$ is the unit tensor, and the second-order mean Eulerian excess pressure $\langle p_2 \rangle$ is given by the difference between the time-averaged acoustic potential and kinetic energy densities [45–47],

$$\langle p_2 \rangle = \langle E_{\text{pot}} \rangle - \langle E_{\text{kin}} \rangle = \frac{1}{2}\kappa_0\langle |p_1|^2 \rangle - \frac{1}{2}\rho_0\langle |\mathbf{v}_1|^2 \rangle. \qquad (10)$$

In the well-known case of a particle suspended in a homogeneous fluid in an acoustic field, the deviation in density and compressibility introduced by the particle leads to a scattered acoustic wave, which induces a divergence $\boldsymbol{\nabla} \cdot \langle \boldsymbol{\Pi} \rangle$ in $\langle \boldsymbol{\Pi} \rangle$. The radiation force exerted on the particle

may then be obtained by integrating the force density $-\boldsymbol{\nabla}\cdot\langle\boldsymbol{\Pi}\rangle$ over a volume enclosing the particle, thereby picking out the divergence at the particle position [18,48].

In the case of an inhomogeneous fluid, the gradient in the continuous material parameters $\rho_0(\boldsymbol{r})$ and $\kappa_0(\boldsymbol{r})$ will likewise lead to a nonzero divergence in $\langle\boldsymbol{\Pi}\rangle$. This is the origin of the acoustic force density $\boldsymbol{f}_{\mathrm{ac}}$ acting on the inhomogeneous fluid at the slow time scale. Consequently, we introduce $\boldsymbol{f}_{\mathrm{ac}}$ as

$$\boldsymbol{f}_{\mathrm{ac}} = -\boldsymbol{\nabla}\cdot\langle\boldsymbol{\Pi}\rangle = -\boldsymbol{\nabla}\langle p_2\rangle - \boldsymbol{\nabla}\cdot\langle\rho_0\boldsymbol{v}_1\boldsymbol{v}_1\rangle. \quad (11)$$

Here, $\langle p_2\rangle$ is given by the local expression (10), which remains true in an inhomogeneous fluid, while the divergence term is rewritten using Eq. (6a) for $\boldsymbol{\nabla}\cdot\boldsymbol{v}_1$ and Eq. (8) defining the mass current potential ϕ_ρ,

$$\boldsymbol{\nabla}\cdot\langle\rho_0\boldsymbol{v}_1\boldsymbol{v}_1\rangle = \langle\boldsymbol{v}_1\cdot\boldsymbol{\nabla}(\rho_0\boldsymbol{v}_1)\rangle + \langle\rho_0\boldsymbol{v}_1(\boldsymbol{\nabla}\cdot\boldsymbol{v}_1)\rangle, \quad (12a)$$

$$= \left\langle\left(\frac{1}{\rho_0}\boldsymbol{\nabla}\phi_\rho\right)\cdot\boldsymbol{\nabla}(\boldsymbol{\nabla}\phi_\rho)\right\rangle + \langle(\boldsymbol{\nabla}\phi_\rho)(\kappa_0\partial_t^2\phi_\rho)\rangle, \quad (12b)$$

$$= \frac{1}{2\rho_0}\boldsymbol{\nabla}\langle|\boldsymbol{\nabla}\phi_\rho|^2\rangle - \kappa_0\langle(\boldsymbol{\nabla}\partial_t\phi_\rho)(\partial_t\phi_\rho)\rangle, \quad (12c)$$

$$= \frac{1}{2\rho_0}\boldsymbol{\nabla}\langle|\boldsymbol{\nabla}\phi_\rho|^2\rangle - \frac{1}{2}\kappa_0\boldsymbol{\nabla}\langle|\partial_t\phi_\rho|^2\rangle, \quad (12d)$$

$$= \frac{1}{2\rho_0}\boldsymbol{\nabla}\langle|\rho_0\boldsymbol{v}_1|^2\rangle - \frac{1}{2}\kappa_0\boldsymbol{\nabla}\langle|p_1|^2\rangle. \quad (12e)$$

In Eq. (12c) we have used $\langle f_1(\partial_t g_1)\rangle = -\langle(\partial_t f_1)g_1\rangle$, valid for time-harmonic fields f_1 and g_1.

Combining Eqs. (9)–(12) and evaluating the time averages [49], we arrive at our final expression for the acoustic force density $\boldsymbol{f}_{\mathrm{ac}}$ acting on an inhomogeneous fluid,

$$\boldsymbol{f}_{\mathrm{ac}} = -\frac{1}{4}|p_1|^2\boldsymbol{\nabla}\kappa_0 - \frac{1}{4}|\boldsymbol{v}_1|^2\boldsymbol{\nabla}\rho_0. \quad (13)$$

This main result, obtained in part by using the mass current potential ϕ_ρ, demonstrates that gradients in compressibility and density lead to a time-averaged acoustic force density acting on an inhomogeneous fluid.

Our theory is consistent with the classical expression for the radiation pressure on an immiscible fluid interface given by the difference in the mean Lagrangian pressure $\langle p_2^L\rangle = \langle E_{\mathrm{pot}}\rangle + \langle E_{\mathrm{kin}}\rangle$ (not the Eulerian pressure $\langle p_2\rangle$) across the interface [45]. Considering a straight interface at $y = 0$ between two immiscible fluids a and b, we may write the fluid property q (either ρ_0 or κ_0) using the Heaviside step function $H(y)$ as $q(y) = q_a + \Delta q H(y)$, where $\Delta q = q_b - q_a$. Integrating $\boldsymbol{f}_{\mathrm{ac}}$ across the interface then yields the force per area $\boldsymbol{F}_{\mathrm{ac}}/A$ on the interface,

$$\frac{\boldsymbol{F}_{\mathrm{ac}}}{A} = -\frac{1}{4}[|p_1|^2\Delta\kappa_0 + |\boldsymbol{v}_1|^2\Delta\rho_0]\boldsymbol{n} = -\Delta\langle p_2^L\rangle\boldsymbol{n}, \quad (14)$$

where $\boldsymbol{n}$ is the normal vector pointing from fluid a to b, and the continuous acoustic fields p_1 and $\boldsymbol{v}_1$ are evaluated at the interface. Inserting into Eq. (14) the explicit expressions for p_1 and $\boldsymbol{v}_1$ in the case of a normally incident wave being partially transmitted from fluid a to fluid b, we recover the radiation pressure given by Lee and Wang [45] in their Eq. (109).

Analytical approximation for $|\hat{\rho}| \ll 1$.—We can obtain analytical results that provide physical insight into the experimentally relevant limit of fluids with a constant speed of sound c and a weakly varying density [37,38]. Writing the latter as $\rho_0(\boldsymbol{r},\tau) = \rho_0^{(0)}[1 + \hat{\rho}(\boldsymbol{r},\tau)]$, where $|\hat{\rho}(\boldsymbol{r},\tau)| \ll 1$ and the superscript (0) indicates zeroth-order in $\hat{\rho}$, we obtain $\boldsymbol{\nabla}\kappa_0 = \frac{1}{c^2}\boldsymbol{\nabla}(1/\rho_0) = -(\kappa_0/\rho_0)\boldsymbol{\nabla}\rho_0$. To first order in $\hat{\rho}$, $\boldsymbol{f}_{\mathrm{ac}}$ in Eq. (13) thus becomes

$$\boldsymbol{f}_{\mathrm{ac}}^{(1)} = \left[\frac{1}{4}\kappa_0^{(0)}|p_1^{(0)}|^2 - \frac{1}{4}\rho_0^{(0)}|\boldsymbol{v}_1^{(0)}|^2\right]\boldsymbol{\nabla}\hat{\rho}. \quad (15)$$

Compared to Eq. (13), this expression constitutes a major simplification since it is linear in $\boldsymbol{\nabla}\hat{\rho}$ and it employs the $\hat{\rho}$-independent homogeneous-fluid fields $p_1^{(0)}$ and $\boldsymbol{v}_1^{(0)}$.

Based on Eq. (15), we demonstrate analytically that our theory is capable of explaining recent experimental results [37,38]. For the system in Fig. 1, with a horizontal acoustic half-wave pressure resonance of amplitude p_{a}, the homogeneous-fluid field solution takes the form,

$$p_1^{(0)} = p_{\mathrm{a}}\sin(ky) \quad \text{with} \quad k = \frac{\pi}{W}, \quad (16a)$$

$$\boldsymbol{v}_1^{(0)} = \frac{p_{\mathrm{a}}}{i\rho_0^{(0)}c}\cos(ky)\boldsymbol{e}_y. \quad (16b)$$

In this case Eq. (15) reduces to

$$\boldsymbol{f}_{\mathrm{ac}}^{(1)} = -\cos(2ky)E_{\mathrm{ac}}^{(0)}\boldsymbol{\nabla}\hat{\rho}, \quad (17)$$

where $E_{\mathrm{ac}}^{(0)} = \frac{1}{4}\kappa_0^{(0)}p_{\mathrm{a}}^2$ is the homogeneous-fluid time-averaged acoustic energy density. Consider a fluid that is initially stratified in horizontal density layers $\hat{\rho}(\boldsymbol{r},0) = \hat{\rho}(z)$ (not the vertical layers seen in Fig. 1), with the dense fluid occupying the floor of the channel ($\partial_z\hat{\rho} < 0$). Equation (17) then predicts that the fluid layers will be pushed downwards near the channel sides, but upwards in the center. This explains the initial phase in the slow-time-scale relocation of the denser fluid to the center of the channel observed experimentally [37].

Slow-time-scale dynamics.—Our experiments confirm the observation [38] that acoustic streaming is suppressed in the bulk of an inhomogeneous fluid. On the slow time scale τ, the dynamics is therefore governed by the acoustic

force density $\boldsymbol{f}_{ac}$, the gravitational force density $\rho_0 \boldsymbol{g}$, and the induced viscous stress, such that the Navier–Stokes equation and the continuity equation take the form

$$\partial_\tau(\rho_0 \boldsymbol{v}) = \boldsymbol{\nabla} \cdot [\boldsymbol{\sigma} - \rho_0 \boldsymbol{v}\boldsymbol{v}] + \boldsymbol{f}_{ac} + \rho_0 \boldsymbol{g}, \qquad (18a)$$

$$\partial_\tau \rho_0 = -\boldsymbol{\nabla} \cdot (\rho_0 \boldsymbol{v}), \qquad (18b)$$

where $\boldsymbol{\sigma}$ is the stress tensor, given by

$$\boldsymbol{\sigma} = -p\mathbf{I} + \eta_0[\boldsymbol{\nabla}\boldsymbol{v} + (\boldsymbol{\nabla}\boldsymbol{v})^T] + \left(\eta_0^b - \frac{2}{3}\eta_0\right)(\boldsymbol{\nabla} \cdot \boldsymbol{v})\mathbf{I}.$$

Here, the superscript T indicates tensor transposition and η_0^b is the bulk viscosity, for which we use the value of water [17]. The inhomogeneity in the fluid parameters is assumed to be caused by a spatially varying concentration field $s(\boldsymbol{r}, \tau)$ of a solute molecule with diffusivity D, satisfying the advection-diffusion equation

$$\partial_\tau s = -\boldsymbol{\nabla} \cdot [-D\boldsymbol{\nabla}s + \boldsymbol{v}s]. \qquad (18c)$$

In our experimental setup, aqueous solutions of iodixanol are used to create inhomogeneities in density, while maintaining an approximately constant speed of sound. The relevant solution properties have been measured as functions of the iodixanol volume-fraction concentration s in our previous work [38]. For the density ρ_0 and viscosity η_0, the resulting fits, valid for $s \leq 0.6$ and $s \leq 0.4$, respectively, are $\rho_0 = \rho_0^{(0)}[1 + a_1 s]$ and $\eta_0 = \eta_0^{(0)}[1 + b_1 s + b_2 s^2 + b_3 s^3]$, with $\rho_0^{(0)} = 1005$ kg/m^3, $\eta_0^{(0)} = 0.954$ mPa s, and $a_1 = 0.522$, $b_1 = 2.05$, $b_2 = 2.54$, $b_3 = 22.8$. The diffusivity was measured *in situ* to be $D = 0.9 \times 10^{-10}$ m^2/s.

Comparison to experiments.—Our experimental setup is described in detail in Ref. [38]. The microchannel in the glass-silicon microchip has the dimensions given in Fig. 1. The horizontal half-wave resonance is excited by driving an attached piezoelectric transducer with an ac voltage U swept repeatedly in frequency from 1.9 to 2.1 MHz in cycles of 1 ms to ensure stable operation. The resulting average acoustic energy density is measured by observing the acoustic focusing of 5 μm beads [50]. The channel inlet conditions are illustrated in Fig. 1: a fluorescently marked 36% iodixanol solution (white) is laminated by 10% iodixanol solutions on either side (black) [51]. The corresponding density variation is 13%, with the maximum at the channel center. At the outlet, after a retention time of $\tau_{ret} = 17$ s, the fluorescence profile is imaged using confocal microscopy in the channel cross section. The characteristic time for diffusion across one third of the channel width is $\tau_{diff} = (1/2D)(W/3)^2 = 87$ s, so diffusion is important but not dominant in the experiment.

We simulate numerically the time evolution in the system using the finite-element solver COMSOL Multiphysics [52], by implementing Eqs. (17) and (18) with the measured dependencies of density $\rho_0(s)$ and viscosity $\eta_0(s)$ on
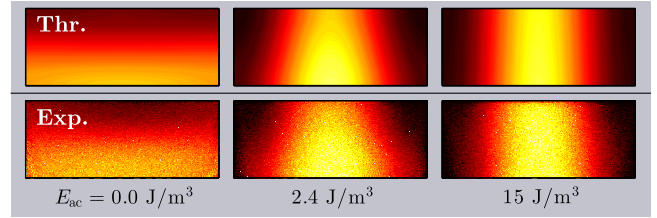

FIG. 2. Theoretical prediction from simulation (top row) and experimental confocal image (bottom row) of the cross-sectional concentration of iodixanol after 17 s retention time for three acoustic energy densities E_{ac}. Initially, the denser fluorescently marked fluid (36% iodixanol, white) is in the center and the less dense fluid (10% iodixanol, black) is at the sides; see Fig. 1. The stable configurations confirm the observation in Ref. [38] that acoustic streaming is suppressed in inhomogeneous fluids. There are no fitting parameters.

concentration s. The initial concentration field $s(\boldsymbol{r}, 0)$ is set to the inlet conditions allowing the concentration field $s(\boldsymbol{r}, \tau_{ret})$ to be compared to the experimental images. The acoustic energy density E_{ac} entering the model is set to the measured experimental value, which leaves no free parameters. Concerning the validity of the numerical solutions, several convergence tests were performed [17], and the integral of s over the domain was conserved in time with a relative error of the order 10^{-3}.

In Fig. 2 we compare the numerically simulated and experimentally measured concentration fields $s(\boldsymbol{r}, \tau)$ at time $\tau_{ret} = 17$ s for three acoustic energy densities E_{ac}. For $E_{ac} = 0$ J/m^3, the initially vertical center fluid column of high density (Fig. 1, white) has collapsed and relocated to the channel bottom due to gravity. For $E_{ac} = 15$ J/m^3, the acoustic force density stabilizes the denser vertical fluid

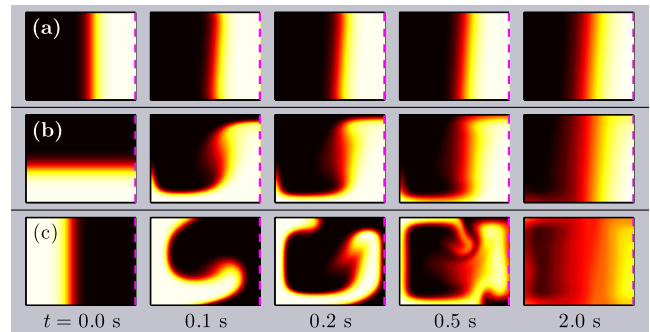FIG. 3. Simulation for $E_{ac} = 10$ J/m^3 of the time evolution of the iodixanol concentration profile in the vertical y-z plane symmetric around $y = 0$ (the dashed line), with only the left half, $-\frac{1}{2}W \leq y \leq 0$, shown. Three different initial configurations of the dense (36% iodixanol, white) and less dense (10% iodixanol, black) solution give rise to different time evolutions. (a) A vertical slab of the dense fluid in the center. (b) A horizontal slab of the dense fluid at the bottom. (c) Two vertical slabs of the dense fluid at the sides. All configurations develop towards a stable configuration, with the dense fluid located as a nearly vertical slab in the center.

column against gravity, such that it broadens only by diffusion. For the intermediate value $E_{ac} = 2.4$ J/m^3, where the gravitational and acoustic forces are comparable, the stable configuration has a triangular shape. Note that the good agreement between the simulated and measured concentration profiles has been obtained without fitting parameters.

In Fig. 3 we show time-resolved simulations obtained with $E_{ac} = 10$ J/m^3 for (a) the stable initial configuration with the denser fluid at the center, (b) the unstable initial configuration with the denser fluid at the bottom, and (c) the unstable initial configuration with the denser fluid at the sides. While the stable initial configuration (a) evolves only by diffusion, the unstable initial configurations (b) and (c) evolve by complex advection patterns into essentially the same stable configuration, with the denser fluid at the center. This fluid relocation is in full qualitative agreement with recent experiments [37]. Movies are provided in the Supplemental Material [53].

Discussion.—Our theory for the acoustic force density acting on an inhomogeneous fluid explains recent experimental observations [37,38] and agrees with our experimental validation without free parameters. The additional observation that steady acoustic streaming, driven by dissipation in the acoustic boundary layers, is suppressed in the bulk of an inhomogeneous fluid [38] has not been treated in this Letter. However, Figs. 2 and 3 demonstrate that the acoustic force density stabilizes a particular inhomogeneous configuration, which suggests that there is a competition between the inhomogeneity-induced acoustic force density (13) and the boundary-driven shear-force density associated with acoustic streaming. The experimental observation of stable inhomogeneous configurations further suggests that the latter is negligible. By adding acoustic boundary layers to our model, we are currently investigating this hypothesis. The extension of acoustic radiation force theory to include inhomogeneous fluids through the introduction of the acoustic force density (13) represents an increased understanding of acousto-fluidics, in general, and further has the potential to open up new ways for microscale handling of fluids and particles using acoustic fields.

————————————

[*]jonkar@fysik.dtu.dk
[†]bruus@fysik.dtu.dk

[1] L. Rayleigh, Philos. Trans. R. Soc. London **175**, 1 (1884).
[2] H. Schlichting, Phys. Z. **33**, 327 (1932).
[3] C. Eckart, Phys. Rev. **73**, 68 (1948).
[4] W. L. Nyborg, J. Acoust. Soc. Am. **30**, 329 (1958).
[5] L. V. King, Proc. R. Soc. A **147**, 212 (1934).
[6] K. Yosioka and Y. Kawasima, Acustica **5**, 167 (1955).
[7] G. Hertz and H. Mende, Z. Phys. **114**, 354 (1939).
[8] K. Bücks and H. Müller, Z. Phys. **84**, 75 (1933).
[9] A. Hanson, E. Domich, and H. Adams, Rev. Sci. Instrum. **35**, 1031 (1964).
[10] D. Foresti, M. Nabavi, M. Klingauf, A. Ferrari, and D. Poulikakos, Proc. Natl. Acad. Sci. U.S.A. **110**, 12549 (2013).
[11] D. Foresti and D. Poulikakos, Phys. Rev. Lett. **112**, 024301 (2014).
[12] A. Marzo, S. A. Seah, B. W. Drinkwater, D. R. Sahoo, B. Long, and S. Subramanian, Nat. Commun. **6**, 8661 (2015).
[13] C. R. P. Courtney, C. E. M. Demore, H. Wu, A. Grinenko, P. D. Wilcox, S. Cochran, and B. W. Drinkwater, Appl. Phys. Lett. **104**, 154103 (2014).
[14] D. Baresch, J.-L. Thomas, and R. Marchiano, Phys. Rev. Lett. **116**, 024301 (2016).
[15] C. E. M. Démoré, P. M. Dahl, Z. Yang, P. Glynne-Jones, A. Melzer, S. Cochran, M. P. MacDonald, and G. C. Spalding, Phys. Rev. Lett. **112**, 174302 (2014).
[16] A. Y. Rednikov and S. S. Sadhal, J. Fluid Mech. **667**, 426 (2011).
[17] P. B. Muller and H. Bruus, Phys. Rev. E **90**, 043016 (2014).
[18] J. T. Karlsen and H. Bruus, Phys. Rev. E **92**, 043010 (2015).
[19] H. Bruus, J. Dual, J. Hawkes, M. Hill, T. Laurell, J. Nilsson, S. Radel, S. Sadhal, and M. Wiklund, Lab Chip **11**, 3579 (2011).
[20] M. Evander, O. Gidlof, B. Olde, D. Erlinge, and T. Laurell, Lab Chip **15**, 2588 (2015).
[21] K. Lee, H. Shao, R. Weissleder, and H. Lee, ACS Nano **9**, 2321 (2015).
[22] F. Petersson, L. Åberg, A. M. Sward-Nilsson, and T. Laurell, Anal. Chem. **79**, 5117 (2007).
[23] M. Wiklund, Lab Chip **12**, 2018 (2012).
[24] D. J. Collins, B. Morahan, J. Garcia-Bustos, C. Doerig, M. Plebanski, and A. Neild, Nat. Commun. **6**, 8686 (2015).
[25] D. Ahmed, A. Ozcelik, N. Bojanala, N. Nama, A. Upadhyay, Y. Chen, W. Hanna-Rose, and T. J. Huang, Nat. Commun. **7**, 11085 (2016).
[26] F. Guo, Z. Mao, Y. Chen, Z. Xie, J. P. Lata, P. Li, L. Ren, J. Liu, J. Yang, M. Dao, S. Suresh, and T. J. Huang, Proc. Natl. Acad. Sci. U.S.A. **113**, 1522 (2016).
[27] B. Hammarström, T. Laurell, and J. Nilsson, Lab Chip **12**, 4296 (2012).
[28] D. Carugo, T. Octon, W. Messaoudi, A. L. Fisher, M. Carboni, N. R. Harris, M. Hill, and P. Glynne-Jones, Lab Chip **14**, 3830 (2014).
[29] G. Sitters, D. Kamsma, G. Thalhammer, M. Ritsch-Marte, E. J. G. Peterman, and G. J. L. Wuite, Nat. Methods **12**, 47 (2015).
[30] P. Augustsson, C. Magnusson, M. Nordin, H. Lilja, and T. Laurell, Anal. Chem. **84**, 7954 (2012).
[31] P. Li, Z. Mao, Z. Peng, L. Zhou, Y. Chen, P.-H. Huang, C. I. Truica, J. J. Drabick, W. S. El-Deiry, M. Dao, S. Suresh, and T. J. Huang, Proc. Natl. Acad. Sci. U.S.A. **112**, 4970 (2015).
[32] B. Hammarström, B. Nilson, T. Laurell, J. Nilsson, and S. Ekström, Anal. Chem. **86**, 10560 (2014).

[33] *Nonlinear Acoustics*, edited by M. F. Hamilton and D. T. Blackstock (Acoustical Society of America, Melville, NY, 2008).

[34] N. Riley, Annu. Rev. Fluid Mech. **33**, 43 (2001).

[35] M. J. Marr-Lyon, D. B. Thiessen, and P. L. Marston, Phys. Rev. Lett. **86**, 2293 (2001).

[36] N. Bertin, H. Chraïbi, R. Wunenburger, J.-P. Delville, and E. Brasselet, Phys. Rev. Lett. **109**, 244304 (2012).

[37] S. Deshmukh, Z. Brzozka, T. Laurell, and P. Augustsson, Lab Chip **14**, 3394 (2014).

[38] P. Augustsson, J. T. Karlsen, H.-W. Su, H. Bruus, and J. Voldman, Nat. Commun. **7**, 11556 (2016).

[39] R. Barnkob, P. Augustsson, T. Laurell, and H. Bruus, Lab Chip **10**, 563 (2010).

[40] P. Augustsson, R. Barnkob, S. T. Wereley, H. Bruus, and T. Laurell, Lab Chip **11**, 4152 (2011).

[41] L. D. Landau and E. M. Lifshitz, *Fluid Mechanics*, 2nd ed., Vol. 6 (Pergamon Press, Oxford, 1993).

[42] P. M. Morse and K. U. Ingard, *Theoretical Acoustics* (Princeton University Press, Princeton, NJ, 1986).

[43] H. Bruus, Lab Chip **12**, 20 (2012).

[44] P. G. Bergmann, J. Acoust. Soc. Am. **17**, 329 (1946).

[45] C. P. Lee and T. G. Wang, J. Acoust. Soc. Am. **94**, 1099 (1993).

[46] B. L. Smith and G. W. Swift, J. Acoust. Soc. Am. **110**, 717 (2001).

[47] L. Zhang and P. L. Marston, J. Acoust. Soc. Am. **129**, 1679 (2011).

[48] Z. Fan, D. Mei, K. Yang, and Z. Chen, J. Acoust. Soc. Am. **124**, 2727 (2008).

[49] The time average of the product of two time-harmonic complex-valued fields f_1 and g_1 is $\langle f_1 g_1 \rangle = \frac{1}{2}\mathrm{Re}[f_1^* g_1]$, where the asterisk denotes complex conjugation.

[50] The average acoustic energy density E_{ac} is estimated as a function of the piezoelectric-transducer voltage U by observing the focusing of 5 μm polystyrene particles in a homogeneous 10% iodixanol solution and comparing to theoretical models; see Refs. [39,40]. In our system, this yields $E_{ac} = kU^2$, with $k = 1.2$ J m^{-3} V^{-2} [38].

[51] We use a fluorescent dextran tracer with the molecular weight of 3000 Da and a diffusivity close to that of iodixanol, which allows indirect visualization of the iodixanol concentration profile; see Ref. [38].

[52] COMSOL Multiphysics 5.2, http://www.comsol.com (2015).

[53] See Supplemental Material at http://link.aps.org/supplemental/10.1103/PhysRevLett.117.114504 for movies of the time evolution of the concentration fields.